9-1998

# Applications of Secondary Electron Energy- and Angular-Distributions to Spacecraft Charging

Neal Nickles

R. E. Davies

## Recommended Citation

Neal Nickles, R.E. Davies and JR Dennison, "Applications of Secondary Electron Energy- and Angular-Distributions to Spacecraft Charging," Proceedings of the 6th Spacecraft Charging Technology Conference, (Air Force Research Laboratory Science Center, Hanscom Air Force Base, MA, 2000).

# Applications of Secondary Electron Energy- and Angular-Distributions to Spacecraft Charging

Neal Nickles, R.E. Davies and J.R. Dennison

Physics Department, Utah State University, Logan

**Abstract**. Secondary electron (SE) emission from spacecraft surfaces as a result of energetic electron bombardment is a key process in the electrical charging of spacecraft. It has been suggested that incorporating more complete knowledge of the energy- and angular-distributions of secondary electrons is necessary to fully model how SE emission and spacecraft charging are affected by re-adsorption of low energy electrons in the presence of charge-induced electrostatic fields and ambient magnetic fields in the spacecraft environment. We present data for such energy- and angular-distributions from sputtered, polycrystalline gold surfaces. The data are compared to empirical SE emission models and found to agree well. We also discuss at what level inclusion of such energy- and angular-distributions will affect models of spacecraft charging for both positive and negative surface charging.

## Introduction

Surfaces of spacecraft materials are exposed to often intense fluxes of charge particles and photons in the space plasma environment. The incident fluxes of charged particles and the fluxes of induced charged particle emission result in spacecraft charging, which can be characterized in terms of a current balance equation as depicted in Figure 1.

Key contributions to the current balance are secondary and backscattered electron emission induced from incident primary electrons, referred to as $J_{2ee}$ and $J_{bse}$ in Figure 1. This paper focuses solely on the effect of the secondary electron current $J_{2ee}$ on charging. A typical distribution of the full range of emitted electrons as a function of emission energy is shown in Figure 2. By convention those emitted electrons having energy $\leq 50$ eV are defined as secondary electrons (SE's); the inset of Figure 2 shows the SE energy-distribution subset of these emitted electrons. The arbitrary division imposed at 50 eV is reasonable because the SE energy-distribution is sharply peaked at low energy ($E_{max} \sim 1$-5 eV [*Seiler 1983*]). For surfaces biased to a voltage $V_{bias}$, we adopt the convention that electrons in the measured spectra with energies $0$ eV $\leq E \leq (50$ eV $- eV_{bias})$ are termed SE's; thus all electrons emitted from the surface as SE's are still considered SE's regardless of the potential difference between the sample and detector.

The secondary electron yield $\delta$ is the total number of secondary electrons emitted per incident primary electron, regardless of emission energy or angle. Current versions of the NASA spacecraft analyzer program NASCAP model the SE contribution to spacecraft charging using only the SE yield as a function of the primary electron's energy and angle of incidence for a given material [*Mandell et al., 1993*]. The SE yield at a fixed incident beam energy can be resolved in terms of the SE's emission energy $E$ or angle $\alpha$. These are expressed as a SE energy-resolved distribution $d\delta(E)/dE$ or an angle-resolved SE distribution $d\delta(\alpha)/d\Omega$. However, this additional information SE emission energy or angle is not currently used in NASCAP charging codes [*Mandell et al., 1993*].

Under certain circumstances, some or all of the emitted SE's are not adsorbed by the ambient plasma, but can return to their surface of origin or to other spacecraft surfaces. These return fluxes can act to alter the current balance equation and ultimately

the charge on the spacecraft. The total SE yield reduced by the return current to the emitting surface is termed the effective SE yield, $\delta_{eff}$. We consider $\delta_{eff}$ rather than the total SE yield, since only SE's that reach the charge sheath or other surfaces are meaningful in determining spacecraft charging. Whether a SE returns to a surface can be influenced by its energy and direction of emission.

The work presented here analyzes the conditions under which information about SE energy- and/or angular-distributions are important in modeling return currents and their concomitant effect on spacecraft charging. A representative set of SE data for gold has been taken. Experimental methods and results are described first. We then consider the effect of the SE energy-distribution on the return current under both positive and negative charging conditions. Subsequently, the angular-distribution is considered. We conclude with a discussion of both distributions in regards to spacecraft charging.
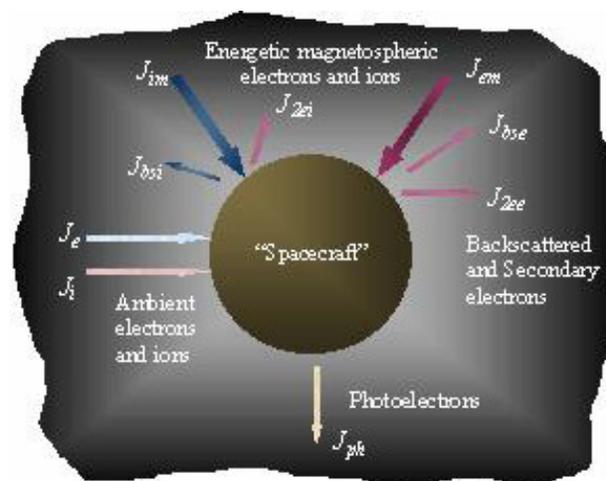


**Figure 1.** Schematic representation of the current balance of incident and emitted fluxes of charged particles that leads to spacecraft charging. The net current density is

$$J_{net} = J_i - J_e + J_{im} - J_{em} + J_{ph} + J_{2ee} + J_{2ei} + J_{bse} = 0$$
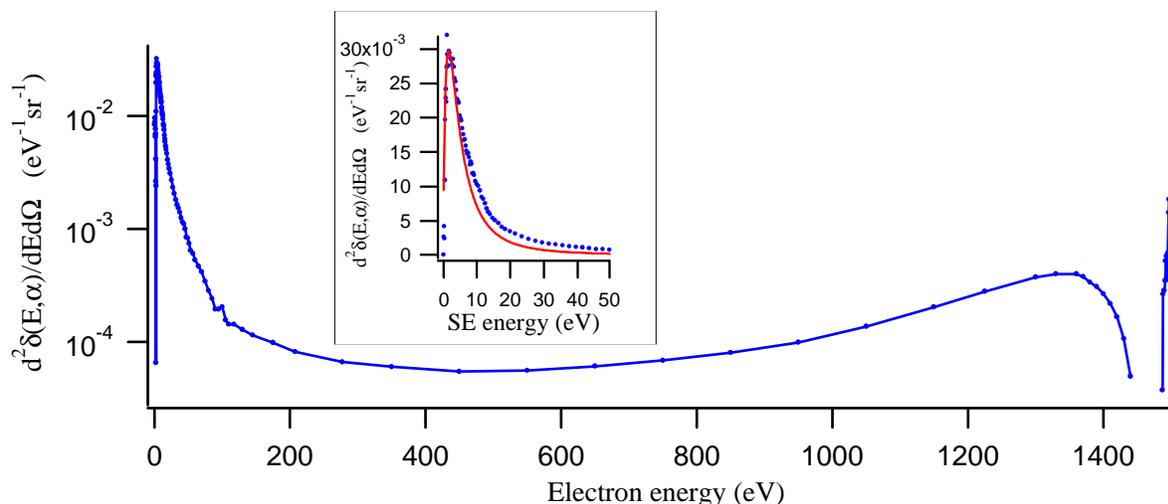
**Figure 2.** Energy-distribution of secondary and backscattered electrons at an emission angle of 17° measured for polycrystalline gold with 1500 eV primary electron beam energy [*Davies, 1999a*]. Note the logarithmic axis for the number of electrons. Inset shows a comparison of the low energy secondary electron energy-distribution (circles) fit with the theoretical model of Eq. 1 (solid line) [*Chung and Everhart, 1974*].

## Experimental Methods

A representative set of energy-, and angular-distribution data was taken for samples of polycrystalline gold. A fixed 1500 eV incident beam energy was used with a 1.5 mm diameter beam spot and a current density of ~$10^{-5}$ A/cm$^2$ at room temperature. To ensure surface cleanliness, the experiments were done in an ultra-high vacuum (UHV) chamber at pressures below $10^{-10}$ torr. Samples were 1 cm$^2$ disks of 99.99% purity gold with surface roughness of <2 μm. The samples were chemically cleaned prior to insertion into the UHV chamber, annealed *in situ* at 200°C for ~12 hr, and sputtered with 500 eV argon ions for ~15 hr to remove surface contamination. Samples were subject to less than ~6 hr of exposure to the electron beam between such *in situ* cleaning. All data and modeling reported here have used an incident beam energy $E_{beam}$=1500 eV and a work function for gold of φ=5.1 eV [*Hölzl et al., 1979*].

SE angular-distributions were measured with a rotatable Faraday cup retarding field analyzer for a range of fixed emission angles between -18° and +73° with respect to the sample normal. The measured energy- and angular-distribution data are shown in Figures 2 and 5, respectively. The effects of an external electrostatic field were studied by applying a negative bias to the sample with respect to the chamber wall (held at ground). Distributions for positive biases are not presented here.

Further details of the instrumentation and experimental procedures are found elsewhere. [*Chang et al., 1999; Davies, 1999a; Davies, 1996*].

## SE Energy-Distribution

Chung and Everhart [*1974*] have derived a semi-empirical theory for the total SE energy-distribution for normal incidence angle that is independent of emission angle

$$\frac{d\delta(E)}{dE} = \frac{k}{E_{beam}} \frac{E}{(E + \phi)^4} \qquad (1)$$

where k is a normalization constant. The inset of Figure 2 shows that this model adequately describes data for our gold samples.

The low energies of the emitted SE's make their trajectories particularly susceptible to fields surrounding a charged spacecraft. In general, the distribution of the SE energies provides information necessary to calculate how the SE population as a whole responds to a given electric and magnetic fields. In this section, we consider electrostatic fields induced by surface charging. The effects of positive and negative charged surfaces on δ are fundamentally different, as shown schematically in Figure 3. In this section, we assume that SE emission is normal to the emitting surface, as is done in existing charging codes. The more physically relevant case, with angular-dependant SE emission, is treated in the next section. To simplify the analysis throughout this paper, electric fields are assumed to be
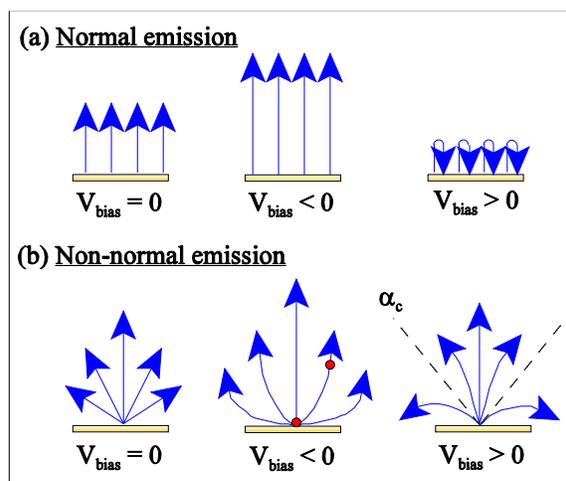


**Figure 3.** The effect of surface charge on SE yield. (a) SE emission normal to the surface and (b) angular-dependant SE emission for: no bias (left), negative bias (center) and positive bias (right).
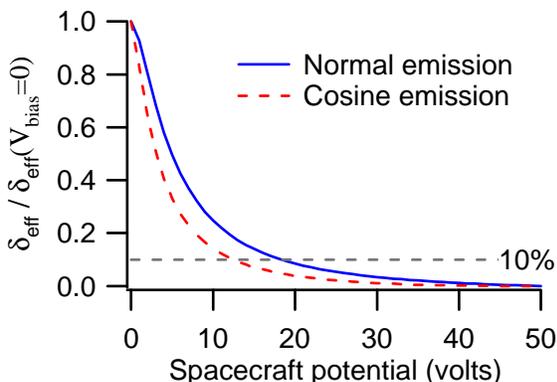
276

**Figure 4.** Effective SE yield (as a percentage of the unbiased SE yield) as a function of positive spacecraft potential for fully normal (solid line) and cosine (dashed line) SE angular-distributions. Sample is polycrystalline gold.



**Figure 5.** SE angle-resolved yield data for polycrystalline Au with $E_{beam}$=1500 eV. The curve fits the data using the cosine distribution of Eq. 3.

normal to the surface.

**Positive Charging**

When a spacecraft surface charges positive with respect to the neutral plasma, the resulting electric field can cause some fraction of the emitted SE's to return to the emitting surface, thereby reducing $\delta_{eff}$.

In the idealized case of fully normal emission [see Figure 3a(right)], the result of a positive bias is to simply shift the SE energy-distribution (see inset of Figure 2) to the left by -e|$V_{bias}$|. A decrease in $\delta_{eff}$ results, since the electrons emitted with energies from 0 eV to +e|$V_{bias}$| no longer escape. Therefore, spacecraft potentials above +50 volts reduce $\delta_{eff}$ of any material to zero. The normalized effective SE yield is plotted as a function of positive potential in Figure 4, where

$$\delta_{eff}\left(V_{bias}\right) = \int_{eV_{bias}}^{50eV} \frac{d\delta(E)}{dE} \cdot dE \qquad (2)$$

Here, we have used the SE energy-distribution for gold shown in Figure 2 and assumed fully normal emission. The SE yield decreases rapidly for |e·$V_{bias}$|>$E_{max}$ and is <10% of the initial SE yield for $V_{bais}$>20 volts≈10 $E_{max}$ for gold.

**Negative Charging**

Negative surface charging produces an electric field which accelerates all SE's leaving the surface. In the idealized case of fully normal emission [see Figure 3a(center)], the result of a negative bias is to shift the SE energy-distribution to the right by +e|$V_{bias}$|. However, $\delta_{eff}$ remains equal to the total SE yield $\delta$ for any negative bias (recall the convention that SE's have energies 0 eV ≤ E ≤ (50 eV - e$V_{bias}$) for surfaces biased to $V_{bias}$).

For more complex scenarios involving multiple surfaces, both positive and negative biases can affect the total electron current balance. The effective SE yield can change in cases of negative bias if the SE's are deflected to another surface (refer to Figure 3b and the next section "SE Angular-Distribution"). Negative bias can enhance absorption of SE's by another surface if the second surface has a higher work function than the emitting
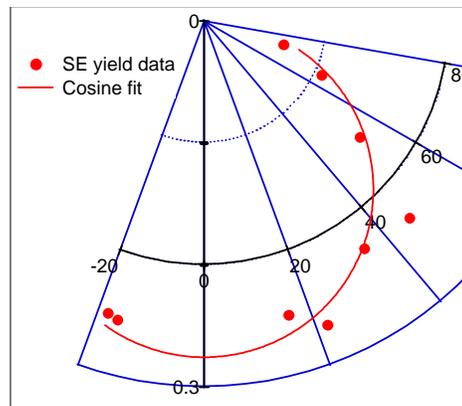
surface. Also, enhanced SE emission due to external electric fields is possible with insulators in special cases. Field emission is unlikely for typical fields produced by spacecraft biases. These more complex effects are discussed elsewhere in more detail [*Davies and Dennison, 1999b*].

## SE Angular-Distribution

The initial SE angular-distribution as SE's leave the emitting surface is predicted to follow a cosine distribution [*Jonker 1951*]

$$\frac{d\delta(\alpha)}{d\Omega} = \delta_o \cos(\alpha) \qquad (3)$$

where $\delta_o$ is the SE yield at $\alpha = 0°$. Figure 5 shows the SE angular-distribution for our polycrystalline gold sample agrees well with Eq. (3).

Surface charging will, in general, alter the trajectories of all SE's, as shown in Figure 3b. This, in turn, will modify the SE angular-distribution at some distance from the emitting surface. Again, we consider both positive and negative bias for normal electric fields.

**Positive Charging**

For positive surface bias, SE's with $p_\perp^2/2m_e < e|V_{bias}|$ are returned to the surface (where $p_\perp$ is the normal momentum component). That is, SE of energy E emitted at $\alpha$ greater than a critical angle $\alpha_C \equiv \cos^{-1}(e|V_{bias}| / E)$ are returned to the surface. Replacing the normal emission distribution with the more realistic angular-dependant distribution of Eq. (3), the effective SE yield as a function of positive surface bias is

$$\delta_{eff}\left(V_{bias}\right) = 2\pi \int_{eV_{bias}}^{50eV} \frac{d\delta(E)}{dE} \left[ \int_0^{\pi/2} \cos(\alpha)\, \Theta[\alpha_c(E) - \alpha] \sin(\alpha)\, d\alpha \right] dE \qquad (4)$$
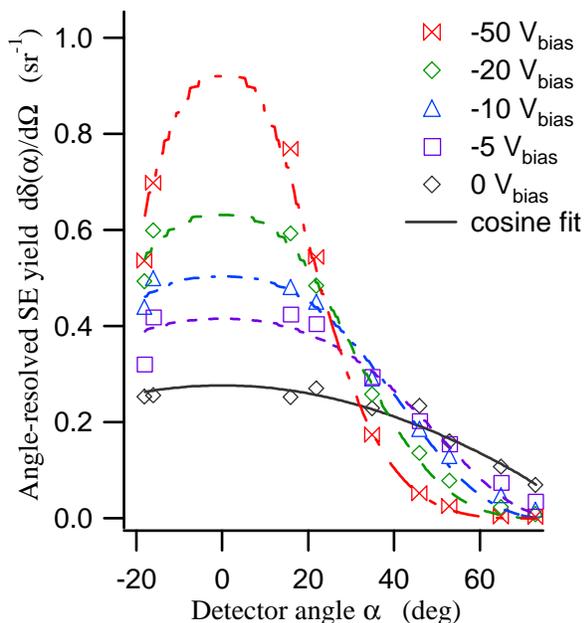
**Figure 6.** Measured angle-resolved SE yield for polycrystalline gold as a function of increasing negative voltage bias on the sample. $E_{beam}$=1500 eV. The solid curve is a fit to the unbiased data using the cosine distribution of Eq. 3. Other curves are guides to the eye.

The Heavyside step function $\Theta(\alpha_C-\alpha)$ models SE re-adsorption. The net effect for any angular-dependant SE distribution is that $\delta_{eff}$ is reduced in comparison to normal emission. For example, $\delta_{eff}(V_{bias})$ is shown in Figure 4, for an energy-distribution given by Eq. 1 fit to the data in the inset of Figure 2 and a cosine angular-distribution given by Eq. 3 fit to the data in Figure 5. The angular-dependant $\delta_{eff}(V_{bias})$ decreases more rapidly than the normal curve and is <10% of the unbiased SE yield for $V_{bias}$>12 volts. Gard [*1973*] did a similar analysis for photoemission data.

**Negative Charging**

A negative bias will repel SE's of all energies, as discussed above, and will also bend all trajectories toward the field lines.
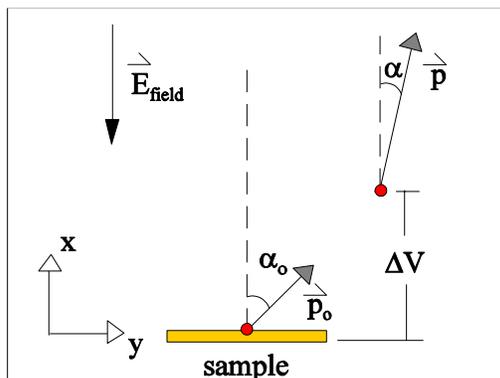


**Figure 7.** Theoretical construct for angular deflection of SE's in electric field $\mathbf{E}_{field}$.
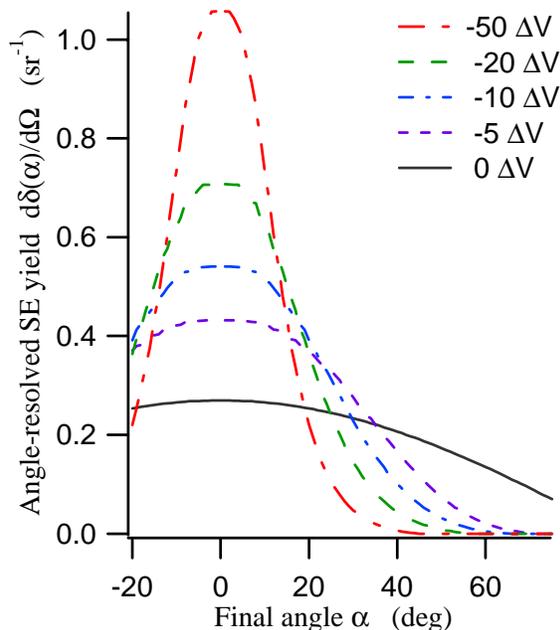


**Figure 8.** Theoretical angle-resolved SE yield as a function of increasing negative potential difference. The solid curve is normalized to agree with the unbiased data of Figure 6.

In essence, the negative bias acts to focus the emitted SE's more in the direction of the electric field, as shown on the middle of Figure 3b.

To investigate the effect of negative sample bias on the SE angular-distribution, we measured this distribution for 5 sample biases in the range 0 V to -50 V. The measured SE angular-distributions, shown in Figure 6, narrow around the sample normal (the assumed direction of the electric field) with increasing negative bias on the sample. Even a small negative bias, on the order of -10 to -20 V, acts to strongly focus the beam toward the normal. We found that the total SE yields were approximately constant, that is the angular integrals of the experimental curves in Figure 6 were approximately constant, varying at most by ±10%.

A simple theoretical model was developed to explain the experimental data shown in Figure 7. Magnetic fields were neglected and the electric fields were assumed to be perpendicular to the sample.

We consider two points along the typical trajectories, indicated as dots in Figures 3b(center) and 7. As shown in Figure 7, an SE emitted with initial angle $\alpha_o$ and initial momentum $p_o$ will be bent into a final angle $\alpha$, as it is accelerated along the electric field lines through a potential difference $\Delta V$. The final angle $\alpha$ can be written in terms of its final momentum as

$$\alpha = \cos^{-1}\left(\frac{p_\perp}{p}\right) \quad (5)$$

The final momentum p and its component perpendicular to the sample $p_\perp$ can be written in terms of their initial values, $p_o$ and $p_{o\perp}$; thus, through conservation of energy, we find

$$\alpha = \cos^{-1}\left(\sqrt{\frac{\left(p_{o_\perp}\right)^2 + 2m_e e\Delta V}{\left(p_o\right)^2 + 2m_e e\Delta V}}\right) \qquad (6)$$

The initial momentum $p_o$ and $p_\perp$ can then be written in terms of the initial energy $E_o$ and angle $\alpha_o$, which yields

$$\alpha = \cos^{-1}\left(\sqrt{\frac{E_o \cos^2\left(\alpha_o\right) + e\Delta V}{E_O + e\Delta V}}\right) \qquad ; \quad 0 \le \alpha_O \le \frac{\pi}{2} \quad (7a)$$

Equation 7(a) is simply a transformation between the initial and final angles $\alpha = \alpha(\alpha_o, E_o; \Delta V)$. Note that the range of possible initial emission angles $0 \le \alpha_o \le \pi/2$ leads to a restriction on the maximum final angle

$$\alpha \le \alpha_{\max} = \cos^{-1}\left(\sqrt{\frac{e\Delta V}{E_O + e\Delta V}}\right) \qquad (7b)$$

The modification of the SE angular-distribution also depends on the SE energy-distribution, since electrons with less energy will undergo a greater angular deflection. Our model assumes that the energy and angular contributions to the SE yield are separable; that is,

$$\frac{d^2\delta(E,\alpha)}{dEd\Omega} = \frac{d\delta(E)}{dE} \cdot \frac{d\delta(\alpha)}{d\Omega} \qquad (8)$$

using Eqs. 1 and 3.

The modified angle-resolved SE yield, $d\delta(\alpha;\Delta V)/d\Omega$, for electrons that have traversed a potential difference $\Delta V$ is found by changing variables from $\alpha_o$ to $\alpha$ in the original cosine distribution (see Eq. 1) and integrating over emission energies $0$ eV$\le E_o \le 50$ eV:

$$\frac{d\delta(\alpha;\Delta V)}{d\alpha} = \int_{0eV}^{50eV} \frac{d\delta(E)}{dE_o} \cos\left[\alpha_o(\alpha, E_o; \Delta V)\right] \frac{d\alpha_o}{d\alpha} \times \qquad (9)$$
$$\Theta\left[\alpha - \alpha_{\max}(E_o; \Delta V)\right] \cdot dE_o$$

The Heavyside step function $\Theta(\alpha - \alpha_{\max}(E_o; \Delta V))$ is included to reflect the restriction in Eq. 7b that $\alpha \le \alpha_{\max}$.

The theoretical angle-resolved SE yields for several potential differences are shown in Figure 8. The normalization constant k for Eq. 1 was chosen so that the solid curves for the unbiased sample in Figures 6 and 8 agreed. This assured that the total SE yields were constant, independent of negative sample bias.

The qualitative similarity of the curve shapes in Figures 6 and 8 is striking. The quantitative differences are minimal, given the simplicity of the theory. The model predicts more peaked distributions with narrower widths and larger maximum yields. Figure 9 illustrates this quantitatively; it shows, as a function of negative potential difference, the angle within which most (arbitrarily chosen as 90%) of the total SE yield is confined.

A primary source of the quantitative disagreement is believed to result from the assumption of the separability of the energy and angular contributions to the SE yield which led to Eq. 8. Further study of this point is in progress [*Davies, 1999a*].

There may also be some difference due to the presence of non-normal or asymmetric electric fields around the sample in the UHV chamber. The assumption that the electric field is perpendicular to the sample is not unreasonable; the flat sample and the cylindrical UHV chamber wall (a geometry similar to a spacecraft surface and the charge sheath) causes the majority of the deflection to occur very near the surface of the sample.
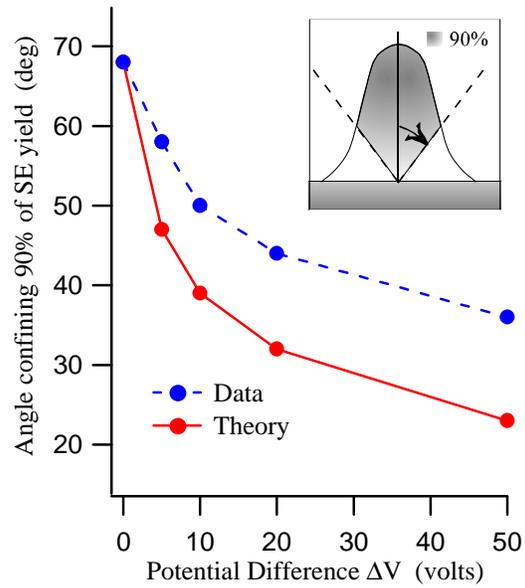


**Figure 9.** Angles that confines 90% of the SE yield of polycrystalline gold as a function of negative potentials difference.

Another source of error may be the perturbing effect of the rotatable detector on these fields as it moves about the sample.

## Application of Results to Spacecraft Charging

The susceptibility of SE's to external fields is seminal in determining the importance of energy- and angle- resolved SE yield information to spacecraft charging. The applicability of the previous analysis to spacecraft charging depends on the specifics of the charging environment. We conclude with a discussion of the question: under what circumstances do we need to consider SE energy- and angular-distributions to adequately model spacecraft charging?

### Magnetic Fields

Magnetic fields can also affect the SE trajectories. The pertinent question is whether magnetic fields encountered in the space environment will cause "significant" angular deflections of SE trajectories in the distances between the emitting surfaces and the plasma sheath. Even larger magnetic fields than those sufficient to "significantly" deflect SE's are required to return SE's to their emitting surface and alter $\delta_{eff}$. An estimate of the effect of magnetic fields found in near-earth orbit environments suggests that even angular deflection needs to be considered only in the most unusual circumstances. The analysis is as follows.

We arbitrarily recognize $\pm 30°$ deflection as "significant". To deviate more than $\pm 30°$ in traversing a distance $L_\perp$ normal to the surface, a 1 eV SE must have a critical orbital radius $r_c \le L_\perp/\sin(30°) = 2 \cdot L_\perp$. We conservatively assume $L_\perp$ is the distance between the spacecraft surface and the charge sheath, which is approximately 1 to 5 times the plasma Debye length $\lambda_D$,

**Table I.** Magnetic Field Parameters for Near-Earth Orbits

| Orbit | Magnetic Field (Gauss) | Larmor radius of 1eV electron $r_L$ (m) | Debye Length $\lambda_D$ (m) | Critical orbital radius $r_c$ (m) |
|---|---|---|---|---|
| GEO | ~0.001 | ~35 | ~10 | 20 to 100 |
| PEO | ≤0.4 | ~0.1 | ~0.01 | 0.02 to 0.1 |
| LEO | ≤0.2 | ~0.2 | ~0.01 | 0.02 to 0.1 |

for low or higher levels of charging, respectively [*Raitt 1999*]. Thus, our criterion for "significant" deflection is that the Larmor radius $r_L$ of a 1 eV SE is less than $r_c$ or 2 to 10 times $\lambda_D$.

We consider typical values for three near-earth orbital environments shown in Table I. In each case, $r_L < r_c$. The only exception is for the case of higher level charging potentials in GEO; however, even extremely weak electrostatic fields completely overwhelm the GEO magnetic field's effect on SE's.

### Electric Fields

For positively charged spacecraft, the analysis leading to Figure 4 allows us to conclude that with positive bias greater than ~5 to 10 $E_{max}$/e (typically 10 to 35 V [*Seiler 1983*]) the effective SE yield is reduced to less than 10% of the initial SE yield. This conclusion is similar for either normal or angular-dependant emission. The suppression of the effective SE yield in such cases serves as negative feedback, minimizing the contribution of $J_{2ee}$ in the current balance equation and decreasing the level of positive charging. A common example of positive spacecraft charging occurs in geosynchronous orbits (GEO), when the spacecraft is in sunlight and the photoelectric yield dominates [*Whipple, 1981*]. Spacecraft potentials in sunlight GEO are typically ~2 volts [*Garrett, 1981*], for which the effective SE yield of gold is reduced by only 35%. In this example, the distance to the plasma sheath over which the 2 volt drop occurs is ~10 m or more (see Table I). Therefore, both energy- and angular-distributions are required to determine if there is significant angular deflection over the length scales of the satellite, which could lead to subsequent absorption by other satellite surfaces or modification of the effective SE yield. Positive charging is not typical of satellites in LEO or PEO.

Negatively charged spacecraft accelerate all SE's leaving the surfaces and typically the effective SE yield does not change appreciably. The concern is that SE's may be subsequently adsorbed by other satellite surfaces, which modifies the current balance equation by effectively increasing $J_e$. The analysis leading to Figure 9 shows that for any negative bias, all SE's will closely follow electric field lines, to within about ±30°, after having traversed a potential difference of about 10 to 40 times $E_{max}$/e (typically 20 to 150 V [*Seiler 1983*]). In GEO, spacecraft in eclipse can reach kilovolt levels of negative absolute or differential charging [*Garrett, 1981*]. Estimating that the kilovolt absolute potential difference occurs over ~10 m, the SE's will follow the field lines after ≥1m. Differential charging may also modify SE trajectories and current collected by other surfaces. In LEO and PEO, the Debye length is ~1 cm, so the initial SE trajectories do not need to be considered at any level of positive or negative charging.

We briefly summarize our most general conclusions as:
- The magnetic field in all earth orbits cannot return SE's to spacecraft; further, no "significant" deflection due to magnetic fields occurs even for low energy 1 eV SE.
- For most common examples of positive charging, the SE yield is not fully suppressed. Given the low positive charging (≲ 100 V) and relatively long Debye lengths in GEO, modeling of SE's adsorbed by other satellite surfaces may require knowledge of SE energy- and angular-distributions.
- For typical examples of negative satellite charging in all environments considered, the total effective SE yield does not change appreciably. However, for lower negative charging (≲200 V) in GEO, modeling of SE's adsorbed by other satellite surfaces may require knowledge of SE energy- and angular-distributions.

### References

Chang, W.Y., R.E. Davies, Neal Nickles and J.R. Dennison, Utah State Univ. ground-based test facility for the study of electronic properties of spacecraft materials, to appear in the Proceedings of 6$^{th}$ Spacecraft Charging Technology Conference, Boston, MA., November 1998.

Chung, M.S. and Everhart T.E., Simple calculation of energy-distribution of low-energy secondary electrons emitted from metals under electron bombardment, *J. Appl. Phys.*, 45, 2, 707-709, 1974.

Davies, R.E., An instrument for experimental secondary electron emission investigations, with application to the spacecraft charging problem, MS Thesis, Utah State University, Logan, Utah, 1996.

Davies, R.E., Measurement of angle-resolved secondary electron spectra, PhD Thesis, Utah State University, 1999a.

Davies, R.E. and J.R. Dennison, Effect of Negative Spacecraft Bias on Secondary Electron Yield, to be submitted, 1999b.

Garrett, H.B., The charging of spacecraft surfaces, *Rev. Geophys. Space Phys.*, 19, 4, 577-616, 1981.

Grard, R.J.L., Properties of satellite photoelectron sheath derived from photoemission laboratory measurements, *J. Geophys. Res.*, 78, 16, 2885-2906, 1973.

Hölzl J. and Schulte, F.K., Work function of metals, in *Solid Surface Physics*, vol. 85, pp. 86, Springer Verlag, 1979.

Jonker, J.H.L., The angular-distribution of the secondary electrons of nickel, *Philips Res. Rep.*, 6, 372-387,1951.

Mandell M.J., P.R. Stannard, and I. Katz, NASCAP programmer's reference manual, NASA Lewis Research Center, May 1993.

Raitt, W.J., personal communication, 1999. Langmuir and Blodgett showed the plasma sheath radius scales approximately linearly with Debye length. Parker and Murphy extended the theory to show that the sheath radius increased with charging potential; typical values were $L_{\_} \approx 5 \lambda_D$. Recent tether experiments show that when motion through the plasma is considered, $L_{\_}$ lies between these extremes.

Seiler, H., Secondary electron emission in scanning electron microscope, *J. Appl. Phys.*,54,1,R1-R18, 1983. A review of the SE energy-distributions of many conducting and insulating materials by Seiler shows that the threshold voltages we determined for gold are fairly representative of most materials. Our stated ranges for the threshold voltages considers a range of values for $E_{max}$/e (1-5 eV) and the FWHM of the SE energy-distribution (4-15 eV).

Whipple, E.C., Potentials of surfaces in space, *Rep. Prog. Phys.*, 44, 1197-1250, 1981.